Pattern Recognition 85 (2019) 37–49

Contents lists available at ScienceDirect

Pattern Recognition

journal homepage: www.elsevier.com/locate/patcog

Mellin polar coordinate moment and its affine invariance

Jianwei Yang[a,*], Liang Zhang[a], Yuan Yan Tang[b]

[a] School of Mathematics and Statistics, Nanjing University of Information Science and Technology, Nanjing 210044 China
[b] Faculty of Science and Technology, University of Macau, Macau, China

ARTICLE INFO

Article history:
Received 5 November 2017
Revised 18 July 2018
Accepted 31 July 2018

Keywords:
Mellin polar coordinate moment
Mellin transform
Repeated integral
Affine moment invariants
Affine transform

ABSTRACT

The moment-based method is a fundamental approach to the extraction of affine invariants. However, only integer-order traditional moments can be used to construct affine invariants. No invariants can be constructed by moments with an order lower than 2. Consequently, the obtained invariants are sensitive to noise. In this paper, the moment order is generalized from integer to non-integer. However, the moment order cannot simply be generalized from integer to non-integer to achieve affine invariance. The difficulty of this generalization lies in the fact that the angular factor owing to shearing in the affine transform can hardly be eliminated for non-integer order moments. In order to address this problem, the Mellin polar coordinate moment (MPCM) is proposed, which is directly defined by a repeated integral. The angular factor can easily be eliminated by appropriately selecting a repeated integral. A method is provided for constructing affine invariants by means of MPCMs. The traditional affine moment invariants (AMIs) can be derived in terms of the proposed MPCM. Furthermore, affine invariants constructed with real-order (lower than 2) MPCMs can be derived using the proposed method. These invariants may be more robust to noise than AMIs. Several experiments were conducted to evaluate the proposed method performance.

1. Introduction

Images of an object captured from different viewpoints are often subject to perspective distortions [1–4]. If the object is small compared to the camera-to-scene distance, the perspective effect becomes negligible and the affine model provides a reasonable approximation of the projective model [2,5]. Therefore, the extraction of affine invariant features plays an important role in object recognition and registration [6–10]. This method has been used extensively in numerous fields, such as shape recognition and retrieval [11,12], watermarking [13], aircraft identification [14,15], texture classification [16], and image registration [17,18].

The moment-based method is the most commonly used technique for the extraction of affine invariant features. However, only integer-order moments can be used to construct affine invariants [4]. It has been reported that high-order moments are sensitive to noise [19]. Hence, in practice, a moment of the lowest possible order should be used [20]. For similarity transform (including only translation, scaling, and rotation), Fourier Mellin descriptors [21] can be viewed as the invariants constructed by complex number order moments. However, similarity transform is only a special case of affine transform [4]. Thus far, an order of moments for constructing affine invariants can only be an integer. In this paper, we consider generalizing the moment order from integer to non-integer, and construct affine invariants by means of the proposed moment.

1.1. Extraction of features invariant to similarity transform by moment

Similarity transform includes translation, scaling, and rotation [4]. Numerous methods for the extraction of similarity invariants are moment-based [22]. The geometric moment of image $Im(x, y)$ is defined as $gm_{pq} = \int\int x^p y^q Im(x,y)dxdy$, where p, q are non-negative integers, and $p+q$ is known as the order of moment gm_{pq}. Then, the central moment μ_{pq} of the image is defined as

$$\mu_{pq} = \int\int (x-x_0)^p (y-y_0)^q Im(x,y)dxdy, \quad (1)$$

where $x_0 = \frac{gm_{10}}{gm_{00}}, y_0 = \frac{gm_{01}}{gm_{00}}$. We note that the geometric moment order is an integer. In this paper, we refer to the central moment as the traditional moment.

The integer order moment has been used extensively to construct similarity invariants. Hu [23] introduced the moment to pattern recognition for the first time and constructed seven similarity invariants with moments of an order less than 3. Since then, the

* Corresponding author.
E-mail addresses: yjianw@nuist.edu.cn (J. Yang), yytang@umac.mo (Y.Y. Tang).

https://doi.org/10.1016/j.patcog.2018.07.036
0031-3203/

rotational moment [24], complex moment [25], and others, have been proposed and used to construct similarity invariants. It was reported in [19] that high-order moments are sensitive to noise. However, moments used in these methods are all of an integer order. Furthermore, the orders of these moments are no less than 2. As a result, methods based on the traditional moment are noise sensitive.

The Fourier Mellin descriptor, proposed by Sheng et al. [21], is the generalization of the traditional moment. This descriptor is defined as follows:

$$M_{s,l} = \int\int r^{s-1} f(r,\theta) e^{il\theta} dr d\theta, \tag{2}$$

where $f(r, \theta)$ is an image expressed in the polar coordinate system and s denotes a complex number. It was also reported in [21] that Hu's moments are special cases of the Fourier Mellin descriptors provided in Eq. (2). Note that the traditional moment in the polar coordinates system can be expressed as follows:

$$\mu_{pq} = \int\int r^{p+q+1} f(r,\theta) \sin^q\theta \cos^p\theta d\theta. \tag{3}$$

Comparing Eqs. (2) and (3), we note that the exponent of r in Eq. (2) is generalized from an integer $p+q+1$ to a complex number $s-1$. That is, the Fourier Mellin descriptor can be viewed as complex number order moment.

Therefore, moment-based methods have been thoroughly developed for the construction of similarity invariants. A moment of any order (even a complex number order) can be used to construct similarity invariants. However, similarity transform is only a special case of affine transform [4]. We consider the problem of constructing affine invariants by means of non-integer order moments in this paper.

1.2. Problems for construction of affine invariants by moment

1.2.1. Construction of affine invariants based on traditional moment

Affine transform provides a reasonable approximation of the projective model [2]; therefore, affine transform and affine invariants are very important in computer vision. Affine transform consists of a linear transformation, as follows:

$$\begin{cases} \tilde{x} = a_{11}x + a_{12}y + b_1, \\ \tilde{y} = a_{21}x + a_{22}y + b_2. \end{cases} \tag{4}$$

The nonsingular matrix $A = \begin{bmatrix} a_{11} & a_{12} \\ a_{21} & a_{22} \end{bmatrix}$ represents the scaling, rotation, and skewing, while $\mathbf{b} = (b_1, b_2)^T$ corresponds to the translation. Similarity transform is simply a special case of affine transform. In fact, when $a_{11} = a_{22}$ and $a_{12} = -a_{21}$, Eq. (4) describes the similarity transform (see [4]).

Affine moment invariants (AMIs) were proposed by Flusser et al. [4,26]. AMIs are the generalization of Hu's moment invariants. Recently, Flusser et al. [27] derived affine invariants by means of graph theory. Using this method, AMIs can be constructed by any integer (no less than 2) order moment. The kernel of these AMIs is defined in terms of the "cross-product" of points $(x_1, y_1) and (x_2, y_2)$ in an image [4,27]:

$$C_{12} = x_1y_2 - x_2y_1. \tag{5}$$

AMIs have been used in numerous fields, such as image registration [4], object recognition [28], and color image processing [29].

As mentioned previously, high-order moments are sensitive to noise. Therefore, the order of moments used to construct affine invariants should be lower in practice. However, AMIs can only be constructed by integer order moments with methods in [4,26], and the lowest order of moments used for constructing AMIs is 2. As a result, AMIs are more sensitive to noise [30].

1.2.2. Need for modification of moment definition

Numerous moment-based methods have been proposed to improve the robustness of affine invariants to noise. In [31], cross-weighted moments were proposed. Although this method overcomes the sensitivity of the moment to noise to a certain degree, it significantly increases the computation amount. Rahtu et al. proposed a series of algorithms for constructing affine invariants by using properties of the random variable function (see, for example, [30,32,33]). In order to improve the recognition rate, additional parameters should be selected. As a result, the computation is greatly increased. Overall, affine invariants based on traditional moments are sensitive to noise. Certain new methods are computationally expensive.

As mentioned previously, AMIs can only be constructed by integer order moments, and two is the lowest order of moments for constructing AMIs. A natural question arises: can we construct affine invariants by means of a moment with an order lower than 2? The zero-order moment gm_{00} is generally used to normalize other quantities to achieve invariance. One-order moments gm_{01}, gm_{10} are generally used to calculate the centroid in order to achieve translation invariance. Therefore, it is impossible to construct invariants with a traditional moment of an order lower than 2. Consequently, the question changes to the following: can we construct affine invariants with non-integer moments? As mentioned previously, the traditional moment order is an integer. Therefore, we need to modify the moment definition so that we can construct affine invariants with moments of an order lower than 2.

1.2.3. Modification difficulties

In the Cartesian system, the integer power of the "cross-product" must be employed to construct affine invariants in order to lower the computational burden. The power of the "cross-product" C_{12} in Eq. (5) is fundamental in affine invariants (see Eq.(3.12) in [4]). Only an integer power of this "cross-product" can enable AMIs to be calculated by a polynomial of moments. For example, an affine invariant with a second-order moment (without normalization), I_1, can be derived as follows (see [4]):

$$I_1 = \int\int\int\int (x_1y_2 - x_2y_1)^2 \prod_{i=1}^{2} Im(x_i, y_i) dx_1 dy_1 dx_2 dy_2 \tag{6}$$

$$= \int\int \left(\int\int x_1^2 Im(x_1, y_1) dx_1 dy_1 \right) y_2^2 Im(x_2, y_2) dx_2 dy_2 + \cdots$$
$$= 2(gm_{20}gm_{02} - gm_{11}^2). \tag{7}$$

We observe from Eq. (6) that I_1 is defined by a quadruple integral. From Eq. (7), we see that I_1 can be calculated by gm_{20}, gm_{02}, and gm_{11}, which are defined by a double integral. Therefore, the computational complexity of AMIs is low. If the power of C_{12} is not an integer (for example, $(C_{12})^2$ is changed to $(C_{12})^{0.5}$ in Eq. (6)), this will result in a quantity that cannot be calculated directly by gm_{pq}. The amount of computation for this is very expensive (see [31]).

In the polar coordinate system, the power for radial factors may differ from the power for the angular part. In the expression of the "cross-product" C_{12}, the radial factors r_1 and r_2 are separated with $\sin(\theta_1 - \theta_2)$:

$$r_1 r_2 sin(\theta_1 - \theta_2). \tag{8}$$

Consequently, the power of the "cross-product" can be generalized into the following form:

$$r_1^{l_1} r_2^{l_2} (\sin(\theta_1 - \theta_2))^{l_3}. \tag{9}$$

Here, it is not necessary for l_3 to be equal to l_1 or l_2. Furthermore, if we employ an integer l_3, the quantity defined in Eq. (9) will result in a polynomial of r_1, r_2, and a certain trigonometric function

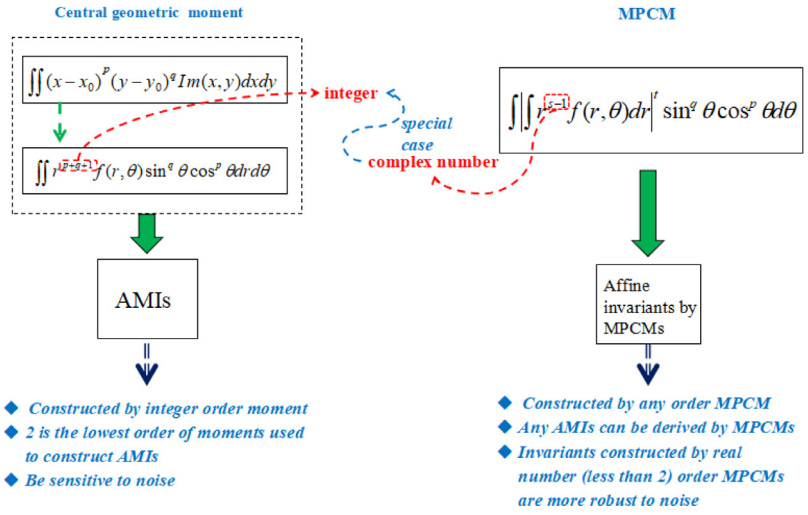

Fig. 1. Main concept of this paper.

of θ_1 and θ_2. As an example, we generalize the quantity provided in Eq. (6) to the following form (l_3 is set as 2):

$$\begin{aligned} PI_1 &= \int\int\int\int r_1^{l_1} r_2^{l_2} (\sin(\theta_1-\theta_2))^2 \prod_{i=1}^{2} f(r_i,\theta_i) r_1 r_2 dr_1 d\theta_1 dr_2 d\theta_2 \\ &= \int\int\int\int r_1^{l_1+1} r_2^{l_2+1} \sin^2\theta_1 \cos^2\theta_2 \prod_{i=1}^{2} f(r_i,\theta_i) dr_1 d\theta_1 dr_2 d\theta_2 + \cdots \qquad (10) \\ &= \left(\int\int r_1^{l_1+1} \sin^2\theta_1 f(r_1,\theta_1) dr_1 d\theta_1\right)\left(\int\int r_2^{l_2+1} \cos^2\theta_1 f(r_2,\theta_2) dr_2 d\theta_2\right) + \cdots \end{aligned}$$

We observe from Eq. (10) that PI_1 is defined with a quadruple integral; however, it can be calculated using a double integral, owing to the integer $l_3 = 2$. Its computational complexity is also low. Therefore, we can generalize the power of the "cross-product" C_{12} to Eq. (9) (l_3 is an integer) for the construction of affine invariants.

However, the definition of the moment should be modified further. In the polar coordinate system, the integral along the radial direction will result in a factor about the angular ($\alpha(\theta)$ in Eq. (20)). In order to achieve affine invariance, this angular factor should be eliminated. As an example, we consider the quantity PI_1 in Eq. (10). Following affine transform, it will be changed to the following $\widetilde{PI}_1$:

$$\widetilde{PI}_1 = \int\int\int\int \tilde{r}_1^{l_1} \tilde{r}_2^{l_2} (sin(\tilde{\theta}_1-\tilde{\theta}_2))^2 \prod_{i=1}^{2} \tilde{f}(\tilde{r}_i,\tilde{\theta}_i) \tilde{r}_1 \tilde{r}_2 d\tilde{r}_1 d\tilde{\theta}_1 d\tilde{r}_2 d\tilde{\theta}_2. \quad (11)$$

It follows from Eqs. (20), (33), and (34) that

$$\widetilde{PI}_1 = (det(A))^8 \int\int\int\int \frac{r_1^{l_1+1} r_2^{l_2+1} (\sin(\theta_1-\theta_2))^2}{(\alpha(\theta_1))^{2-l_1} (\alpha(\theta_2))^{2-l_2}} \prod_{i=1}^{2} f(r_i,\theta_i) dr_1 d\theta_1 dr_2 d\theta_2. \qquad (12)$$

We compare Eq. (10) with (12). In order to ensure that $\widetilde{PI}_1$ is a relative affine invariant of PI_1, we should set l_1 and l_2 to be equal to 2. As a result, PI_1 in Eq. (10) is the same as I_1 in Eq. (6). Consequently, no further affine invariants will be constructed by generalizing the power of the "cross-product" to Eq. (9). Simply generalizing the moment from integer to non-integer is of no use.

1.3. Contributions and organization of this paper

In this paper, the moment order is generalized from integer to non-integer. The Mellin polar coordinate moment (MPCM) is proposed and a method is provided for constructing affine invariants. The main concept is illustrated in Fig. 1. The contributions of this paper are listed as follows.

- The MPCM, the order of which is a complex number, is proposed.

The order of the traditional moment is an integer, but high-order moments are sensitive to noise [19]. We generalize the traditional moment so that the moment order can be a non-integer. However, the moment order cannot simply be generalized to a non-integer. The traditional moment is defined by a double integral. In the polar coordinate system, a repeated integral is employed to calculate the traditional moment. However, the integral along the radial direction will result in an angular factor $\alpha(\theta)$ owing to the shearing in the affine transform (see $\alpha(\theta)$ in Eq. (20)). In order to eliminate this angular factor, only high-order moments can be employed to construct affine invariants. The MPCM proposed in this paper is defined directly by a repeated integral (see top right in Fig. 1). By using an appropriate repeated integral (the power t in the definition of MPCM), the factor $\alpha(\theta)$ by the integral along the radial direction can easily be eliminated. As a result, non-integer order (even for complex number order) moments can be used to construct the affine invariants. The traditional moment is only a special case of the proposed MPCM.

Mellin transform has been used for the extraction of invariant features [34–39]. However, features extracted by these methods are only invariants to similarity transform. In this paper, we propose the MPCM to extract affine invariants by employing Mellin transform.

- A method is provided for constructing affine invariants by means of MPCM.

The MPCM is defined by a repeated integral, and affine invariants can be constructed by moments of any order. Based on the MPCM, the method for constructing affine invariants is presented in this paper. As the MPCM is the generalization of the traditional moment, all AMIs can be derived by means of the proposed method. Furthermore, we provide several affine invariants constructed by real-order MPCMs. The experimental results verify the affine invariance of the invariants constructed by MPCMs.

• The invariants constructed by lower real-order MPCMs are robust to noise.

High-order traditional moments are sensitive to noise [19]. A low-order moment should be used to extract invariant features. However, the order of the traditional moment used to construct affine invariants is no less than 2. With the MPCM, the moment order is generalized from an integer to a non-integer. As a result, moments with real number (lower than 2) orders can be used to construct affine invariants. We conduct several experiments to test the robustness of these invariants to noise. Certain Chinese characters, English capital letters, the Coil-20 database and various images in ILVRC2012 are used as test images. The results demonstrate that the invariants constructed by low real-order (less than 2) MPCMs are more robust to noise.

The remainder of this paper is organized as follows. In Section 2, MPCM is introduced. In Section 3, a method is presented for the extraction of affine invariants by means of MPCM. Thereafter, we construct several affine invariants using the proposed method. Meanwhile, we explain that affine invariants constructed by traditional moments are only special cases of invariants constructed by MPCMs. The proposed method performance is evaluated experimentally in Section 4. Finally, concluding remarks are provided in Section 5.

2. Mellin polar coordinate moment

Let h be a 1D function. The Mellin transform of h is a function defined by [40]:

$$M_h(s) = \int h(x)x^{s-1}dx, \tag{13}$$

where $s = \sigma + i\tau$. The real part σ of s is a constant, selected so that the integral in Eq. (13) converges. The imaginary part τ of s is the transform variable.

In order to define the MPCM, the Cartesian coordinate system should first be converted into the polar coordinate system. The origin of the reference system is translated into the image centroid. We denote the image as $f(r, \theta)$ in the polar coordinate system, in which a point (x, y) can be described as $x = r\cos\theta, y = r\sin\theta$, $\theta \in [0, 2\pi)$, and $r = \sqrt{x^2+y^2}$, where r represents the distance between point (x, y) and the image centroid.

Definition 1. The MPCM of image $f(r, \theta)$ is defined as follows:

$$M(s,t,p,q) = \int \left| \int r^{s-1} f(r,\theta)dr \right|^t \sin^q\theta\cos^p\theta d\theta, \tag{14}$$

where $s = \sigma + i\tau$ ($\sigma \geq 1$), p, q, t are non-negative real numbers, and $s-2$ is known as the order of the MPCM.

Remark 1. The MPCM is the generalization of the traditional moment.

According to Definition 1, the central moment can be expressed by the MPCM:

$$\mu_{pq} = \int \left[\int r^{p+q+1} f(r,\theta)dr \right] \sin^q\theta\cos^p\theta d\theta = M(p+q+2, 1, p, q).$$

That is, the MPCM is the generalization of the traditional moment.

Remark 2. The MPCM is defined in terms of a repeated integral.

As mentioned previously, μ_{pq}, the traditional moment, is defined by a double integral. In the polar coordinate system, μ_{pq} is calculated by a repeated integral. The integral along the radial direction results in an angular factor $\alpha(\theta)$ in Eq. (20). High-order traditional moments are employed in order to eliminate this factor. In this paper, the MPCM is directly defined by a repeated integral (see Eq. (14)). Consequently, the angular factor $\alpha(\theta)$ provided in Eq. (20) can be eliminated by selecting an appropriate t in Eq. (14).

Remark 3. The MPCM can be viewed as complex number order moment.

The traditional moment order is an integer (p, q in Eq. (3) are all integers). Using the traditional method, only moments with orders no less than 2 can be used to construct affine invariants. However, s in Eq. (14) is a complex number, and an integer is only a special case of a complex number. Therefore, the MPCM can be viewed as a complex number order moment.

Furthermore, the MPCM exhibits the following property.

Theorem 1. *For $s_1 = \sigma + \tau i, s_2 = \sigma - \tau i,\ t \in \mathbb{R}^+$ and any non-negative real numbers p, q, the following equation holds:*

$$M(s_1,t,p,q) = M(s_2,t,p,q). \tag{15}$$

Proof.

$$\begin{aligned} M(s_1,t,p,q) &= \int \left| \int e^{(s_1-1)lnr} f(r,\theta)dr \right|^t \sin^q\theta\cos^p\theta d\theta \\ &= \int \left| \int e^{(\sigma-1)lnr+i\tau lnr} f(r,\theta)dr \right|^t \sin^q\theta\cos^p\theta d\theta \\ &= \int \left| \int e^{(\sigma-1)lnr-i\tau lnr} f(r,\theta)dr \right|^t \sin^q\theta\cos^p\theta d\theta \\ &= M(s_2,t,p,q) \end{aligned}$$

This completes the proof. □

3. Construction of affine invariants by MPCMs

In this section, we provide a general method for the extraction of affine invariant features based on the MPCM. Firstly, the affine transformation in the polar coordinate system is briefly reviewed in Section 3.1. Thereafter, a general method is presented for constructing affine invariants by MPCMs in Section 3.2. In Section 3.3, we construct several affine invariants using the proposed method. We demonstrate that affine invariants constructed by traditional moments [4,27] are only special cases of invariants constructed by MPCMs. Furthermore, we construct several affine invariants by MPCMs with orders that are real numbers.

3.1. Affine transformation in polar coordinate system

In order to achieve translation invariance, the reference system origin is translated into the image centroid, as mentioned previously. Consequently, the relation of Eq. (4) can be expressed as follows:

$$\tilde{\boldsymbol{x}} = \boldsymbol{A}\boldsymbol{x}. \tag{16}$$

Suppose that the Cartesian coordinate system has been converted into the polar coordinate system, in which a pair of affine-related points (x, y) and $(\tilde{x}, \tilde{y})$ in the Cartesian coordinate system can be described as follows:

$$\begin{cases} x = r\cos\theta \\ y = r\sin\theta \end{cases}, \qquad \begin{cases} \tilde{x} = \tilde{r}\cos\tilde{\theta} \\ \tilde{y} = \tilde{r}\sin\tilde{\theta} \end{cases} \tag{17}$$

where $\theta, \tilde{\theta} \in [0, 2\pi)$, $r = \sqrt{x^2+y^2}$, and $\tilde{r} = \sqrt{\tilde{x}^2+\tilde{y}^2}$.

According to Eqs. (16) and (17), we obtain the following equations:

$$\begin{cases} \tilde{r}\cos\tilde{\theta} = a_{11}r\cos\theta + a_{12}r\sin\theta \\ \tilde{r}\sin\tilde{\theta} = a_{21}r\cos\theta + a_{22}r\sin\theta \end{cases} \tag{18}$$

It follows that

$$\tilde{r} = r\sqrt{(a_{11}\cos\theta + a_{12}\sin\theta)^2 + (a_{21}\cos\theta + a_{22}\sin\theta)^2},$$

and

$$\tan\tilde{\theta} = \frac{\tilde{y}}{\tilde{x}} = \frac{a_{21}\cos\theta + a_{22}\sin\theta}{a_{11}\cos\theta + a_{12}\sin\theta}.$$

We set

$$\alpha(\theta) = \sqrt{(a_{11}\cos\theta + a_{12}\sin\theta)^2 + (a_{21}\cos\theta + a_{22}\sin\theta)^2},$$
$$\beta(\theta) = \frac{a_{21}\cos\theta + a_{22}\sin\theta}{a_{11}\cos\theta + a_{12}\sin\theta}. \tag{19}$$

It follows that

$$\tilde{r} = \alpha(\theta)r, \tag{20}$$

$$\tan\tilde{\theta} = \beta(\theta). \tag{21}$$

From Eq. (18), we know that

$$\cos\tilde{\theta} = \frac{a\cos\theta + b\sin\theta}{\alpha(\theta)}, \quad \sin\tilde{\theta} = \frac{c\cos\theta + d\sin\theta}{\alpha(\theta)}. \tag{22}$$

3.2. Method for constructing affine invariants

In this subsection, we provide a method for constructing affine invariants by means of the MPCM. Firstly, we obtain the following result.

Theorem 2. *Select $g \in \mathbb{Z}^+$, $s_i = \sigma_i + i\tau_i$ $(\sigma_i \geq 1)$, and $m_{jk} \geq 0$ $(j, k = 1, \cdots, g)$. Furthermore, let $m_{jk} = 0$ $(1 \leq j \leq k \leq g)$. Set*

$$t_i = \frac{1}{\sigma_i}\left(\sum_{j=i+1}^{g} m_{ji} + \sum_{k=1}^{i-1} m_{ik} + 2\right), \tag{23}$$

$$n = \sum_{g\geq j>k\geq 1} m_{jk} + g. \tag{24}$$

Then, the following quantity is an affine invariant:

$$I = \frac{1}{M^n(2,1,0,0)} \int\int\cdots\int \prod_{i=1}^{g} \left| \int r_i^{s_i-1} f(r_i,\theta_i) dr_i \right|^{t_i} \prod_{g\geq j>k\geq 1} \sin(\theta_k - \theta_j)^{m_{jk}} d\theta_1 d\theta_2 \cdots d\theta_g. \tag{25}$$

We provide the proof of Theorem 2 in Appendix A.

In the above theorem, m_{jk} is only a non-negative real number. Therefore, $sin(\theta_k - \theta_j)^{m_{jk}}$ may not be expressed in a polynomial of $sin\theta_k$, $cos\theta_k$, $sin\theta_j$, and $cos\theta_j$. As a result, I in Eq. (25) may not be expressed by the MPCM. In the following theorem, we restrict m_{jk} to be an integer. Consequently, a method is provided for constructing affine invariants by means of the MPCM.

Theorem 3. *Select $g \in \mathbb{Z}^+$, $g \geq j > k \geq 1$. Let $s_i = \sigma_i + i\tau_i$ $(\sigma_i \geq 1)$. Set $m_{jk} \geq 0$ $(j, k = 1, \cdots, g)$ to be non-negative integers. Furthermore, if $1 \leq j \leq k \leq g$, let $m_{jk} = 0$. Set t_i $(i = 1, \cdots, g)$, and n as in Eqs. (23) and (24). Then, the following quantity is an affine invariant:*

$$I = \frac{1}{M^n(2,1,0,0)}\left(\sum_{Q_{jk}=0}^{m_{jk}} \prod (-1)^{\sum(m_{jk}-Q_{jk})} C_{m_{jk}}^{Q_{jk}} \prod_{i=1}^{g} M(s_i, t_i, p_i, q_i)\right), \tag{26}$$

for $i = 1, \cdots, g$, p_i and q_i are provided by the following equations:

$$p_i = \sum_{j=i+1}^{g} Q_{ji} + \sum_{k=1}^{i-1}(m_{ik} - Q_{ik}), \tag{27}$$

$$q_i = \sum_{j=i+1}^{g} (m_{ji} - Q_{ji}) + \sum_{k=1}^{i-1} Q_{ik}. \tag{28}$$

We provide the proof of Theorem 3 in Appendix A.

Theorem 3 provides the method for constructing affine invariants by means of MPCMs. In the following subsection, we employ this method to construct affine invariants.

3.3. Affine invariants constructed by MPCMs

In this subsection, we apply the method provided in Theorem 3 to construct affine invariants. Firstly, we drive several AMIs listed in [4,27] by means of Theorem 3. These invariants are constructed by traditional moments with integer orders. Thereafter, we construct certain affine invariants using MPCMs with real-number orders.

3.3.1. Derivation of certain AMIs

As mentioned previously, traditional moments are only special cases of the MPCM. Therefore, AMIs, which are constructed by traditional moments, can be derived using Eq. (26). The following three AMIs were provided by Flusser et al. [4,27] (we denote these by *AMI*1, *AMI*2, and *AMI*3, respectively):

$$\begin{aligned} AMI1 &= \frac{\mu_{20}\mu_{02} - \mu_{11}^2}{\mu_{00}^4}, \\ AMI2 &= \frac{\mu_{30}^2\mu_{03}^2 - 6\mu_{30}\mu_{21}\mu_{12}\mu_{03} + 4\mu_{30}\mu_{12}^3 + 4\mu_{21}^3\mu_{03} - 3\mu_{21}^2\mu_{12}^2}{\mu_{00}^{10}}, \\ AMI3 &= \frac{\mu_{20}(\mu_{21}\mu_{03} - \mu_{12}^2) - \mu_{11}(\mu_{30}\mu_{03} - \mu_{21}\mu_{12}) + \mu_{02}(\mu_{31}\mu_{12} - \mu_{21}^2)}{\mu_{00}^7}. \end{aligned} \tag{29}$$

We derive these using Theorem 3.

In fact, if we set $g = 2, s_1 = s_2 = 4$, and $m_{21} = 2$, it follows from Eq. (26) that

$$AMI1 = \frac{2}{M^4(2,1,0,0)}\big(M(4,1,2,0)M(4,1,0,2) - M^2(4,1,1,1)\big). \tag{30}$$

In other words, *AMI*1 can be derived by MPCMs.

Similarly, we can derive *AMI*2 and *AMI*3 by means of Eq. (26). We put the derivation of *AMI*2 and *AMI*3 in Appendix B. In fact, any AMIs constructed using traditional moments can be derived by MPCMs.

That is, we generalize the traditional moments from an integer order to a non-integer order. Theorem 3 is in fact the generalization of the method for constructing AMIs.

3.3.2. Affine invariants with real-order MPCMs

AMIs [4,27] are constructed by traditional moments with integer orders. The lowest order for constructing AMIs is 2 (see Eq. (29), AMI1 is constructed by two order moments u_{02}, u_{20}, u_{11}). Affine invariants cannot be constructed using traditional moments with orders of less than 2. In contrast, the order of a MPCM can be a real number. Consequently, we can construct affine invariants using moments with orders that are real numbers less than 2. These invariants may be more robust to noise than AMIs. Here, we provide a method for constructing affine invariants with real-order MPCMs.

In Theorem 3, if we set s_i to be a real number $(s_i \geq 1)$, we obtain the method for constructing affine invariants by means of real-order MPCMs. Here, we set $g = 2, m_{jk} = 2$, $s_1 \geq 1$ and $s_2 \geq 1$. Then,

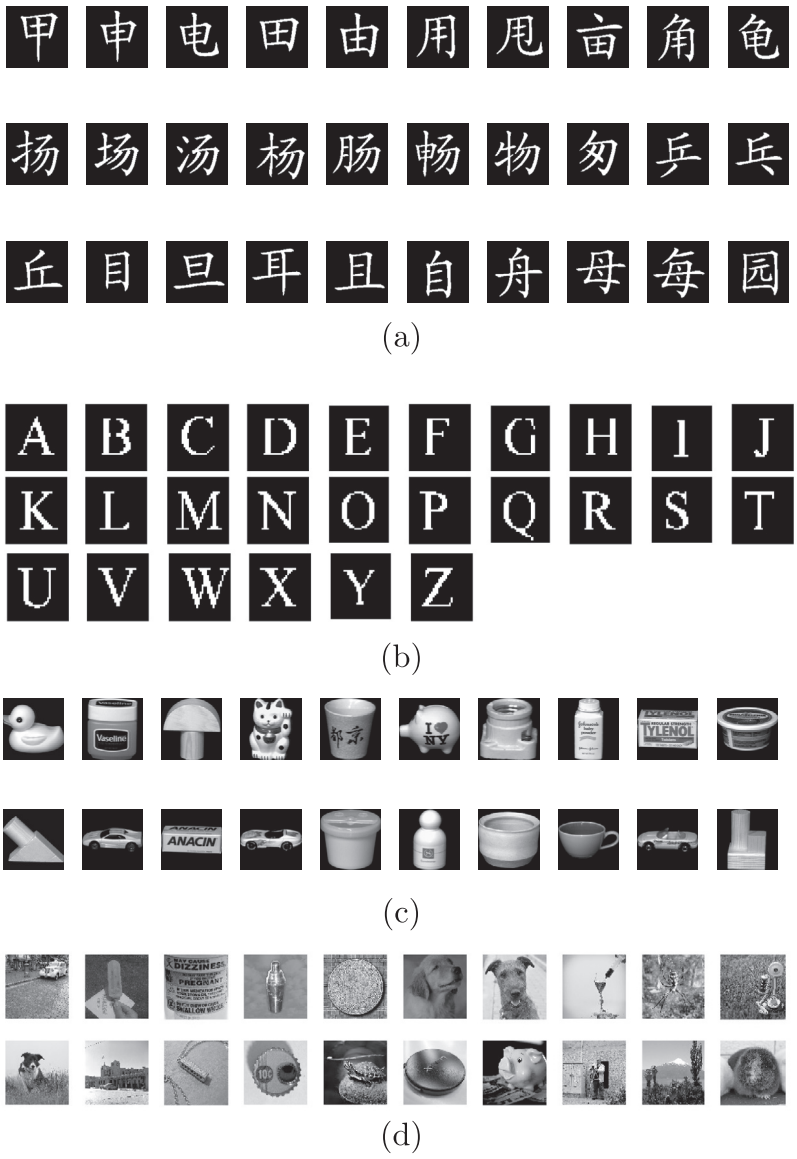

Fig. 2. (a) 30 Chinese characters, (b) 26 English capital letters, (c) Columbia Coil-20 images, and (d) 20 images from ILSVRC2012.

we obtain the following invariant:

$$I=\frac{\int\int\left|\int r_1^{s_1-1}f(r_1,\theta_1)dr_1\right|^{\frac{4}{s_1}}\left|\int r_2^{s_2-1}f(r_2,\theta_2)dr_2\right|^{\frac{4}{s_2}}sin(\theta_1-\theta_2)^2d\theta_1d\theta_2}{[\int\int rf(r,\theta)drd\theta]^4}. \tag{31}$$

This can be written in terms of the MPCM based on Theorem 3, as follows:

$$\begin{aligned} I=&\frac{1}{M^4(2,1,0,0)}(M(s_1,\frac{4}{s_1},2,0)M(s_2,\frac{4}{s_2},0,2)\\ &+M(s_1,\frac{4}{s_1},0,2)M(s_2,\frac{4}{s_2},2,0)\\ &-2M(s_1,\frac{4}{s_1},1,1)M(s_2,\frac{4}{s_2},1,1). \end{aligned} \tag{32}$$

We observe that I in Eq. (32) is the same as AMI1 provided in Eq. (30) if we set $s_1=s_2=4$. If we set $1\le s_1, s_2<4$, s_1-2 and s_2-2 are less than 2. Consequently, the orders of MPCMs in Eq. (32) are less than 2. As mentioned previously, no affine invariants can be constructed by traditional moments with orders less than 2. Using Eq. (32), we can construct affine invariants by means of Theorem 3, using MPCMs with orders of less than 2. In Section 4, we use Eq. (32) to extract invariants, and the experimental results demonstrate that these invariants are more robust than AMIs to noise.

4. Experiments

In this section, we test the proposed method performance. Four groups of images are used as the test database. The performance on binary images is tested using the images in Fig. 2(a) and (b). Fig. 2(a) includes 30 Chinese characters with *regular script font*, and these images have a size of 128×128. Fig. 2(b) includes all of the English capital letters with *Times New Roman font*, and the size of each letter is 256×256. The Columbia Coil-20 database [41] (Fig. 2(c)) is used to test the performance on gray-scale images. The backgrounds of the images in the above three databases are clean. In order to make the situation challenging, we test the proposed method performance on 20 images from ILSVRC2012 [42] (see Fig. 2(d)). In Section 4.1, we verify the affine invariance of the constructed invariants. We compare the computational complexity of the MPCM with traditional moments in Section 4.2. Fi-

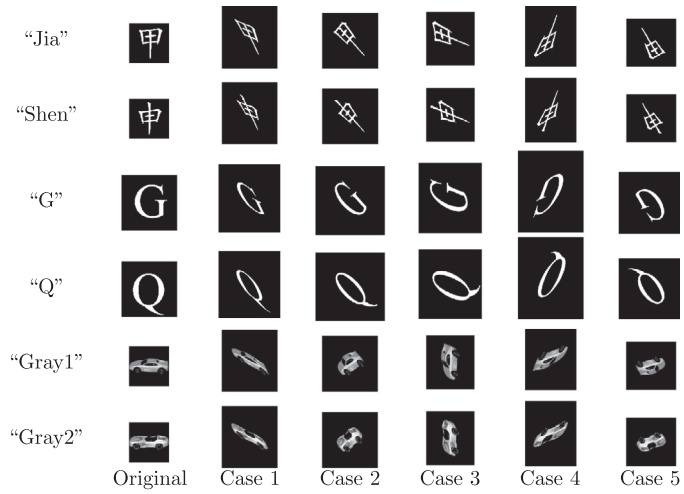

Fig. 3. Images before and after affine transformation.

Table 1
The feature $I_{1.5}^{1.5}$ extracted from the images in Fig. 3.

	Original	Case 1	Case 2	Case 3	Case 4	Case 5
"Jia" ($\times 10^{-6}$)	7.8518	7.7369	7.7903	7.8024	7.6299	7.6771
"Shen" ($\times 10^{-6}$)	8.6192	8.5372	8.4459	8.5427	8.4824	8.5208
"G" ($\times 10^{-7}$)	7.9160	7.9520	7.9407	7.9719	7.9374	7.9446
"Q" ($\times 10^{-7}$)	8.4227	8.3725	8.3858	8.3895	8.4634	8.4496
"Gray1"	0.0040	0.0041	0.0041	0.0041	0.0041	0.0041
"Gray2"	0.0057	0.0056	0.0057	0.0056	0.0056	0.0056

nally, we test the robustness of the affine invariants constructed by real-order MPCMs to noise in Section 4.3.

4.1. Affine invariance

In order to verify the affine invariance of the invariants constructed by Theorem 3, the experimental results for two groups of invariants are presented in this subsection. The first group is composed of two invariants constructed by real-order MPCMs, which are derived by setting $g = 2$ and $m_{21} = 2$ in Theorem 3. Moreover, s_1 and s_2 are selected as $s_1 = 1.5$, $s_2 = 1.5$ and $s_1 = 2.5$, $s_2 = 3.0$, respectively. These two invariants are denoted by $I_{1.5}^{1.5}$ and $I_{2.5}^{3.0}$ for the sake of convenience. The second group is composed of two invariants constructed by imaginary-order MPCMs. We set $g = 2$ and $m_{21} = 2$ in Theorem 3 and select two sets of parameters: $s_1 = 1.0 + 1.5i$, $s_2 = 1.0 + 4.0i$ and $s_1 = 1.0 + 2.0i$, $s_2 = 1.0 + 3.0i$, respectively. These two invariants are denoted by $I_{1.0+1.5i}^{1.0+4.0i}$ and $I_{1.0+2.0i}^{1.0+3.0i}$, respectively. Three groups of images and their affine transformation images are used to test the affine invariance (see Fig. 3). The first group of images consists of two similar Chinese characters, "Jia" and "Shen", as illustrated in Fig. 2(a). These two Chinese characters are similar in structure; only partially different. The second group of images consists of two similar English capital letters, "G" and "Q", in Fig. 2(b). The third group of images consists of two similar gray images in Fig. 2(c), denoted by "Gray1" and "Gray2".

The results of these four affine invariants are displayed in Tables 1–4. From these results, we can observe that the invariants constructed by MPCMs are affine invariants. Moreover, different objects often exhibit varying features, despite their structures being similar, such as "Jia" and "Shen".

4.2. Computational complexity

We compare the computational efficiency of MPCM with that of the traditional moment by means of experiments. We employ the 20 gray images in Fig. 2(c) with different sizes for this test. The sizes of these images are adjusted to 64×64, 128×128, $\cdots$, and 640×640, respectively.

Firstly, we test the computation times for the calculation of a MPCM and a traditional moment. Here, we only list the results for traditional moments with $p = 2$ and $q = 1$ in Eq. (1), and MPCMs with $s = 3$, $t = 1$, $p = 1$, and $q = 1$ in Eq. (14) (similar results are obtained for other parameters). Table 5 presents the average times for 20 images with different sizes. From this table, we can observe that the MPCM requires slightly more time than the traditional moment (owing to the coordinate transform) for small-size images. As the size increases, the MPCM calculation speed approaches that of the traditional moment. As mentioned previously, the MPCM is directly defined by a repeated integral (see Eq. (14)). Consequently, the MPCM may theoretically exhibit the same computational complexity as that of the traditional moment.

Thereafter, we test the computation times for calculating an invariant by means of MPCM and by means of the traditional moment (AMI1). We list the results for the traditional moment with AMI1, and the invariant by means of MPCM with $s_1 = 1.5, s_2 = 2.5$, and $m_{21} = 2$ in Eq. (26) (the results are similar for other invariants). Table 6 presents the average times for 20 images with different sizes. We observe that the computation time of the invariant by means of MPCM is greater than that of AMIs for images of small sizes. However, the computation time of the invariant by means of MPCM is smaller than that of the AMIs for images with large sizes.

4.3. Performance of affine invariant with real-order MPCM against noise

In this paper, we generalize the traditional moment from the integer to non-integer order. It was reported in [19] that high-order moments are sensitive to noise. The order of the traditional moment used to construct the affine invariant is only an integer that is no less than 2. In this paper, real-order MPCMs with orders of less than 2 can be used to construct affine invariants. In this subsection, we test the robustness of invariants using real-order (less than 2) MPCMs to noise.

In order to discuss the robustness of invariants constructed by MPCMs to noise, the relative error is defined to measure the difference between the invariant of the original and noised images. The relative error is defined as follows:

$$E(I, \tilde{I}) = \frac{\|I - \tilde{I}\|}{\|I\|},$$

where I and $\tilde{I}$ represent the invariants extracted from the original and noised images, respectively, while $\|\cdot\|$ represents the Euclidean norm.

AMI1 is the affine invariant constructed using the lowest-order traditional moment (the order is 2). For the sake of comparison with the traditional moment, we set $g = 2$, $m_{21} = 2$ in Theorem 3 and construct affine invariants with various s_1 and s_2, as described in subsection 3.3.2.

4.3.1. Performance of affine invariant in binary images

As the binary image only has two values, namely 0 and 1, we only test the robustness of this image to Salt & Pepper noise. Firstly, we select a binary image displaying the Chinese character "Jia" in Fig. 2(a) as the test image. The other binary image exhibits similar results (see Fig. 5). We add Salt & Pepper noise with the intensity set to 0.03 to this binary image (see Fig. 4(a)). Moreover, s_1 and s_2 vary from 1 to 6, and the step length is set to 0.2. As the noise is random, we record the average of 50 tests. The results are displayed in Fig. 4(b), and the following facts can be observed.

- In general, the relative error will increase with increasing s_1 and s_2 within the region $\{(s_1, s_2) \mid s_1 + s_2 < 4, s_1 \geq 1, s_2 \geq 1\}$ (in a

Table 2
The feature $I_{2.5}^{3.0}$ extracted from the images in Fig. 3.

	Original	Case 1	Case 2	Case 3	Case 4	Case 5
"Jia" ($\times 10^{-6}$)	5.0891	5.0786	5.0571	5.0773	4.9911	5.0492
"Shen" ($\times 10^{-6}$)	4.5715	4.5626	4.5331	4.6223	4.5541	4.5666
"G" ($\times 10^{-6}$)	5.2230	5.3415	5.3414	5.3093	5.3412	5.3444
"Q" ($\times 10^{-6}$)	4.9494	4.9467	4.9557	4.9367	4.9588	4.9482
"Gray1" ($\times 10^{-9}$)	6.2411	6.2500	6.2520	6.2510	6.2509	6.2499
"Gray2" ($\times 10^{-9}$)	5.6913	5.6801	5.6785	5.6742	5.6782	5.6791

Table 3
The feature $I_{1.0+1.5i}^{1.0+4.0i}$ extracted from the images in Fig. 3.

	Original	Case 1	Case 2	Case 3	Case 4	Case 5
"Jia" ($\times 10^{-7}$)	1.7741	1.8468	1.9148	1.7016	1.7849	1.8377
"Shen" ($\times 10^{-7}$)	2.1909	2.3991	2.2321	2.3171	2.4373	2.1877
"G" ($\times 10^{-8}$)	9.5382	9.2252	9.2104	9.3212	9.2270	9.2207
"Q" ($\times 10^{-8}$)	9.6513	9.5360	9.5609	9.6092	9.6843	9.7504
"Gray1"	52.8549	48.2271	48.2127	47.4189	47.7799	48.2819
"Gray2"	57.7545	56.2940	51.8988	54.3771	57.7729	52.1590

Table 4
The feature $I_{1.0+2.0i}^{1.0+3.0i}$ extracted from the images in Fig. 3.

	Original	Case 1	Case 2	Case 3	Case 4	Case 5
"Jia" ($\times 10^{-7}$)	1.0055	0.9271	0.9511	0.9383	0.8844	0.9270
"Shen" ($\times 10^{-7}$)	1.2489	1.1289	1.2379	1.2770	1.0923	1.2300
"G" ($\times 10^{-7}$)	1.1067	1.0671	1.0561	1.0795	1.0675	1.0665
"Q" ($\times 10^{-7}$)	1.1188	1.1053	1.1078	1.1147	1.1232	1.1302
"Gray1"	76.3832	69.6025	71.2137	71.1419	70.5615	70.4280
"Gray2"	64.8341	62.3518	65.8400	63.1210	62.2727	63.6968

Table 5
Computational time (in s) of traditional moment and MPCM for images of different sizes.

	64×64	128×128	256×256	384×384	512×512	640×640
AMI1	0.0037	0.0057	0.0179	0.0409	0.0853	0.1389
MPCM	0.0134	0.0245	0.0504	0.0764	0.1048	0.1354

Table 6
Computational time (in s) for AMI1 and invariant by means of MPCM for images of different sizes.

	64×64	128×128	256×256	384×384	512×512	640×640
AMI1	0.0044	0.0101	0.0406	0.1077	0.2738	0.4112
Invariant by MPCM	0.0275	0.0533	0.1064	0.1584	0.2203	0.2809

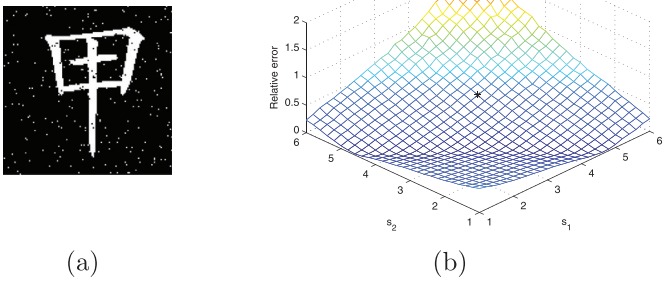

Fig. 4. (a) noised binary image, (b) relative error with different s_1 and s_2 (the black "*" represents the result for $s_1 = s_2 = 4$ (AMI1)).

less strict sense). Moreover, it will decrease with increasing s_1 and s_2 within the region $\{(s_1, s_2) \mid s_1 + s_2 < 4, s_1 \geq 1, s_2 \geq 1\}$ (in a less strict sense). The relative error will reach its minimum near the line $s_1 + s_2 = 4$.

- The affine invariants constructed by MPCMs with (s_1, s_2) in the region $\{(s_1, s_2) | 1 \leq s_1 < 4, 1 \leq s_2 < 4\}$ are more robust to noise than AMI1 (marked by "*" in the image).

As mentioned previously, the traditional moment can be viewed as special case of the proposed MPCM. AMI1 is the invariant constructed by the traditional moment with the lowest order of 2, and corresponds to the invariants constructed by MPCM with $s_1 = 4$ and $s_2 = 4$. As reported in [19], a higher-order moment is more sensitive to noise for the traditional moment. Therefore, AMI1 is more robust to noise than the other AMIs. From Fig. 4(b), we observe that the relative error of AMI1 is greater than that of the affine invariants constructed by MPCMs with (s_1, s_2) in the region $\{(s_1, s_2) | 1 \leq s_1 < 4, 1 \leq s_2 < 4\}$. Consequently, the AMIs are more sensitive to noise than the invariants constructed by MPCMs with (s_1, s_2) in the region $\{(s_1, s_2) | 1 \leq s_1 < 4, 1 \leq s_2 < 4\}$.

In order to compare the performance of the invariants by means of real-order MPCMs with those of AMI1, AMI2, and AMI3 in terms of quantity, we add various intensities of Salt & Pepper noise to the above-mentioned binary image "Jia". The noise intensity is set to 0.01, 0.02, ⋯, and 0.06. The relative errors are denoted by E_1^s, E_2^s, ⋯, and E_6^s, respectively. Furthermore, we record the average value of 50 tests. Several values of s_1 and s_2 are used for the test $(s_1, s_2 \geq 1)$. The results are listed in Table 7, including those for AMI1, AMI2, and AMI3. From Table 7, we can observe that the affine invariants with low real-order $(1 \leq s_1 < 4, 1 \leq s_2 < 4)$ MPCMs are more robust to Salt & Pepper noise than the invari-

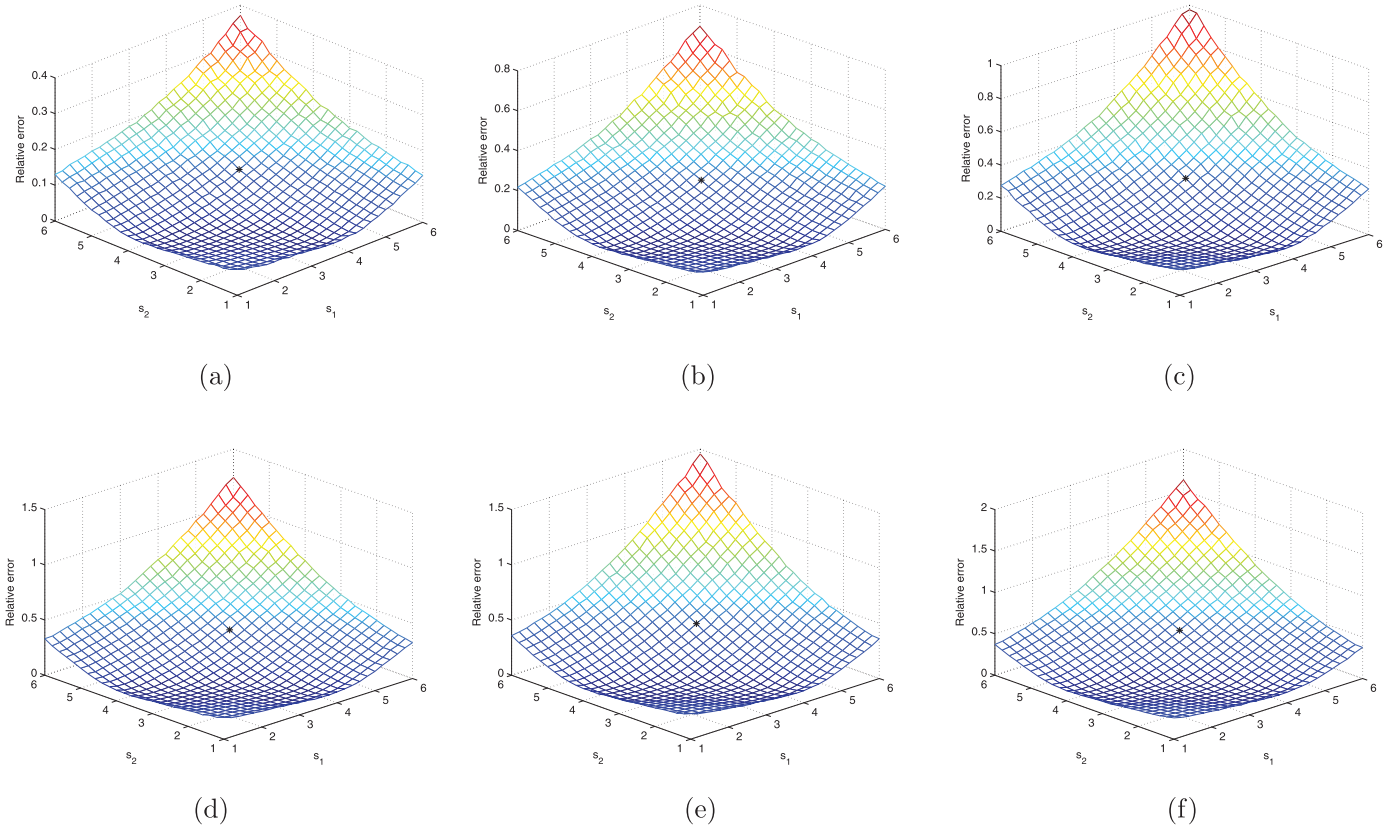

Fig. 5. From (a) to (f): average relative errors of 30 binary images with Salt & Pepper noise of different intensities (the black "*" represents the result for $s_1 = s_2 = 4$ (AMI1)).

Table 7
Relative errors of affine invariants under different degrees of Salt & Pepper noise for Chinese character "Jia".

	E_1^s	E_2^s	E_3^s	E_4^s	E_5^s	E_6^s
s_1, s_2						
1.0, 1.0	0.1818	0.3381	0.4452	0.5304	0.5843	0.6329
1.1, 1.2	0.1506	0.2941	0.3880	0.4696	0.5254	0.5710
1.4, 1.4	0.1265	0.2265	0.3101	0.3800	0.4398	0.4781
1.5, 1.5	0.1135	0.2076	0.2864	0.3536	0.4057	0.4457
1.5, 2.2	0.0830	0.1504	0.2167	0.2679	0.3119	0.3506
2.0, 2.5	0.0532	0.0966	0.1388	0.1734	0.2036	0.2237
2.5, 2.5	0.0371	0.0608	0.0855	0.1127	0.1313	0.1486
3.0, 3.0	0.0112	0.0190	0.0280	0.0349	0.0405	0.0442
3.2, 3.4	0.0408	0.0780	0.1167	0.1417	0.1559	0.1870
*AMI*1	0.1688	0.3254	0.4471	0.5639	0.6318	0.7180
*AMI*2	0.6557	1.0988	1.3573	1.4478	1.5336	1.5780
*AMI*3	0.2119	0.4527	0.6353	0.8202	0.9218	1.0343

Table 8
Average relative errors of 30 Chinese characters with Salt & Pepper noise.

	E_1^s	E_2^s	E_3^s	E_4^s	E_5^s	E_6^s
s_1, s_2						
1.0, 1.0	0.0763	0.1200	0.1627	0.1946	0.2280	0.2582
1.1, 1.2	0.0606	0.0978	0.1339	0.1604	0.1953	0.2227
1.4, 1.4	0.0492	0.0781	0.1088	0.1394	0.1692	0.1934
1.5, 1.5	0.0466	0.0737	0.1023	0.1318	0.1606	0.1837
1.5, 2.2	0.0381	0.0599	0.0809	0.1016	0.1234	0.1421
2.0, 2.5	0.0305	0.0439	0.0580	0.0706	0.0821	0.0935
2.5, 2.5	0.0282	0.0377	0.0480	0.0577	0.0655	0.0730
3.0, 3.0	0.0339	0.0450	0.0548	0.0561	0.0720	0.0810
3.2, 3.4	0.0500	0.0771	0.1000	0.1228	0.1400	0.1554
*AMI*1	0.1122	0.2026	0.2849	0.3514	0.4039	0.4467
*AMI*2	1.1617	2.2315	2.8412	4.0415	4.3884	4.9111
*AMI*3	0.2676	0.4496	0.5883	0.7352	0.8516	0.9373

ants with an order of two ($s_1 = s_2 = 4$) MPCMs (AMI1). As s_1 or s_2 varies from 1 to 4, the robustness to noise of the constructed invariants first increases and then decreases. Compared to AMIs, the invariants constructed by the MPCM with orders lower than 2 are more robust to Salt & Pepper noise than AMI1, AMI2, and AMI3. That is, the affine invariants constructed by low-order MPCMs exhibit stronger robustness. In the following experiment, further binary images of Chinese characters are tested.

In order to illustrate the performance of invariants constructed by real-order MPCMs further, 30 binary images of Chinese characters, illustrated in Fig. 2(a), are used as test images. Salt & Pepper noise with an intensity set to 0.01, 0.02, ⋯, and 0.06 is added to each binary image of Chinese characters. Here, s_1 and s_2 vary from 1 to 6, and the step length is also set to 0.2. Each result represents the average value of the relative error of 30 binary images (the result of each binary image is the average value of 10 tests). The results are illustrated in Fig. 5, from which we observe that the affine invariants constructed by real-order MPCMs exhibit stronger robustness to Salt & Pepper noise when s_1 and s_2 are relatively small.

Similarly, we compare the performances of the invariants constructed by real-order MPCMs with those of AMI1, AMI2, and AMI3 in terms of quantities, and list the results in Table 8. Salt & Pepper noise with an intensity set to 0.01, 0.02, ⋯, and 0.06, respectively, is also added to each binary image of Chinese characters in Fig. 2(a). The relative errors are again denoted by E_1^s, E_2^s, ⋯, and E_6^s. The relative error of 30 binary images is averaged and listed in Table 8. From Table 8, we can also observe that the affine invariants with low real-order ($1 \le s_1 < 4$, $1 \le s_2 < 4$) MPCMs are more robust to Salt & Pepper noise than invariants with two-order ($s_1 = s_2 = 4$) MPCMs (AMI1). As s_1 or s_2 varies from 1 to 4, the robustness to noise of the constructed invariants first increases and then decreases. Compared to the AMIs, the invariants constructed by MPCMs with orders lower than 2 are more robust to Salt & Pep-

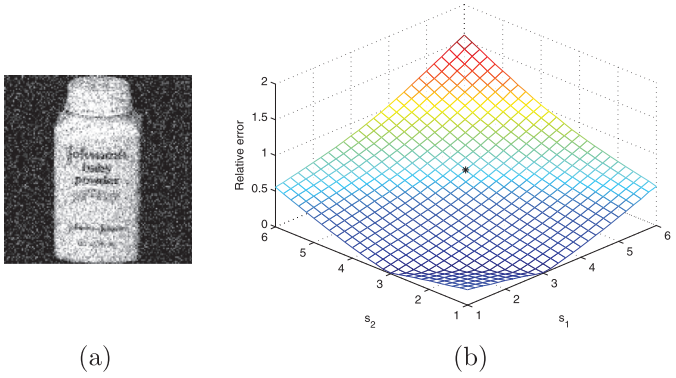

Fig. 6. (a) Noised gray image, and (b) relative error with different s_1 and s_2 (the black "*" represents the result for $s_1 = s_2 = 4$ (AMI1)).

per noise than AMI1, AMI2, and AMI3. Hence, the affine invariants constructed by low-order MPCMs exhibit stronger robustness.

The results of the 26 English capital letters in Fig. 2(b) are similar to those of the 30 Chinese characters in Fig. 2(a), and we omit these here.

4.3.2. Performance of affine invariant in gray images

In order to test the robustness of affine invariants constructed by real-order MPCMs for gray images, the images in Fig. 2(c) are used as test images. The test process is similar to that for the binary images in the above subsection. We test the performance of invariants in these images for Salt & Pepper noise and Gaussian noise. We only list the results for the Gaussian noise in order to avoid redundancy. The results for the Salt & Pepper noise are similar.

Firstly, we select a gray image (denoted by "Gray3") in Fig. 2(c) as the test image (other images yield similar results). We add Gaussian noise with a mean value set to 0 and intensity set to 0.03 to this image (see Fig. 6(a)). The results for other intensities are similar. The s_1, s_2 values also vary from 1 to 6, and the step length is set to 0.2. The results are illustrated in Fig. 6(b). Similarly, we record the average value of 50 tests. From Fig. 6(b), it can be observed that the affine invariants constructed by real-order MPCMs exhibit stronger robustness to Gaussian noise when s_1 and s_2 are relatively small ($s_1 < 4$, $s_2 < 4$). With an increase of s_1 and s_2 used to construct the affine invariants, the robustness of the affine invariants will decrease.

For the gray image "Gray3", we compare the performance of the invariants constructed by real-order MPCMs for Gaussian noise to those of AMI1, AMI2, and AMI3 in terms of quantity. We add Gaussian noise with a mean value of 0 and intensity set to 0.01, 0.02, ⋯, and 0.06, respectively. The relative errors are denoted by E_1^g, E_2^g, ⋯, and E_6^g. We also record the average value of 50 tests. Different values of s_1 and s_2 are used for the test ($s_1, s_2 \geq 1$). The results are listed in Table 9, including those for AMI1, AMI2, and AMI3. By Table 9, we can observe that the affine invariants with low real-order ($1 \leq s_1 < 4$, $1 \leq s_2 < 4$) MPCMs are more robust to Gaussian noise than those with two-order ($s_1 = s_2 = 4$) MPCMs (AMI1). As s_1 or s_2 varies from 1 to 4, the robustness to noise of the constructed invariants first increases and then decreases. Compared to the AMIs, the invariants constructed by MPCM with orders lower than 2 are more robust to Gaussian noise than AMI1, AMI2, and AMI3. That is, the affine invariants constructed by low-order MPCMs exhibit stronger robustness to Gaussian noise.

In order to avoid the special case, we conduct experiments on the gray images in Fig. 2(c). Gaussian noise with a mean value of 0 and intensity set to 0.01, 0.02, ⋯, and 0.06, respectively is added to each gray image. Moreover, s_1 and s_2 vary from 1 to 6, and the step length is also set to 0.2. We use Fig. 7 to demonstrate the average relative error values for 20 gray images in Fig. 2 (c) (the result of each image is the average value of 10 tests). It can be observed from Fig. 7 that the affine invariants constructed by real-

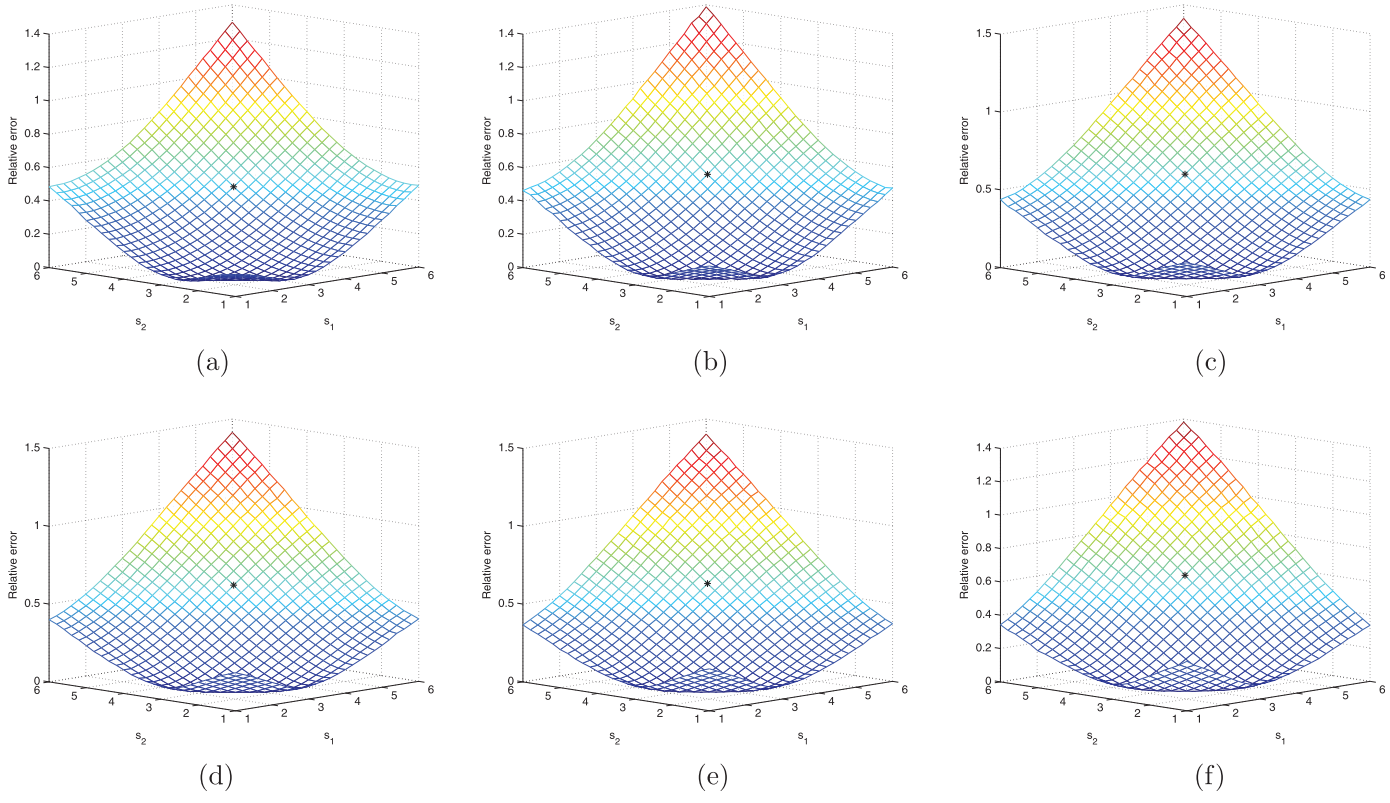

Fig. 7. From (a) to (f): average relative errors of 20 gray images in Fig. 2(c) for Gaussian noise with different intensities (the black "*" represents the result for $s_1 = s_2 = 4$ (AMI1)).

Table 9
Relative errors of affine invariants under different degrees of Guassian noise for gray image "Gray3".

	E_1^g	E_2^g	E_3^g	E_4^g	E_5^g	E_6^g
s_1, s_2						
1.0, 1.0	0.1175	0.1732	0.2163	0.2602	0.2830	0.3096
1.1, 1.2	0.1015	0.1487	0.1852	0.2177	0.2420	0.3607
1.4, 1.4	0.0766	0.1105	0.1340	0.1557	0.1752	0.1892
1.5, 1.5	0.0674	0.0995	0.1166	0.1352	0.1499	0.1625
1.5, 2.2	0.0287	0.0388	0.0475	0.0537	0.0593	0.0638
2.0, 2.5	0.0181	0.0282	0.0371	0.0436	0.0500	0.0557
2.5, 2.5	0.0502	0.0734	0.0926	0.1076	0.1228	0.1353
3.0, 3.0	0.1301	0.1850	0.2251	0.2593	0.2871	0.3142
3.2, 3.4	0.1881	0.2617	0.3157	0.3587	0.3985	0.4347
*AMI*1	0.3667	0.4928	0.5868	0.6608	0.7243	0.7816
*AMI*2	1.0400	1.2300	1.2667	1.3144	1.3318	1.3342
*AMI*3	0.7219	0.8985	0.9717	0.9843	1.0158	1.0405

Table 10
Average of relative errors of 20 images in Fig. 2(d) for different Gaussian noise levels.

	E_1^g	E_2^g	E_3^g	E_4^g	E_5^g	E_6^g
s_1, s_2						
1.0, 1.0	0.0164	0.0300	0.0437	0.0566	0.0702	0.0841
1.1, 1.2	0.0114	0.0209	0.0309	0.0407	0.0504	0.0606
1.4, 1.4	0.0062	0.0118	0.0173	0.0230	0.0286	0.0342
1.5, 1.5	0.0049	0.0093	0.0137	0.0183	0.0227	0.0270
1.5, 2.2	0.0030	0.0055	0.0080	0.0103	0.0126	0.0147
2.0, 2.5	0.0026	0.0047	0.0069	0.0089	0.0110	0.0129
2.5, 2.5	0.0029	0.0057	0.0086	0.0115	0.0145	0.0174
3.0, 3.0	0.0045	0.0088	0.0133	0.0180	0.0226	0.0270
3.2, 3.4	0.0053	0.0104	0.0158	0.0211	0.0265	0.0318
*AMI*1	0.0070	0.0135	0.0204	0.0272	0.0340	0.0407
*AMI*2	0.1374	0.2318	0.3092	0.3699	0.4143	0.4590
*AMI*3	0.1149	0.2023	0.3258	0.4378	0.5405	0.6232

order MPCMs exhibit stronger robustness to Gaussian noise when s_1 and s_2 are relatively small ($s_1 < 4$, $s_2 < 4$).

Here, we also compare the performances of the invariants constructed by real-order MPCMs with those of AMI1, AMI2, and AMI3 in terms of quantities for Gaussian noise. Gaussian noise with a mean value of 0 and intensities set to 0.01, 0.02, $\cdots$, and 0.06, respectively is added to each gray image in Fig. 2(c) and (d). The relative errors are also denoted by E_1^g, E_2^g, $\cdots$, and E_6^g. For each image, we take the average value of 50 tests. Then, the relative errors of 20 gray images in Fig. 2 (d) are averaged and listed in Table 10. The results for the images in Fig. 2 (c) are similar, and we omit these here. From Table 10, we can also observe that the affine invariants constructed by low-order MPCMs exhibit stronger robustness.

In summary, the affine invariants constructed by low real-order (less than 2) MPCMs are more robust to noise than invariants constructed by traditional moments. When using the traditional method, affine invariants can only be constructed by integer-order moments, and the lowest moment order used to construct invariants is 2. As a result, invariants by traditional moments are sensitive to noise. By using the proposed method, invariants can be constructed with any order MPCMs, and invariants with low real-order MPCMs are more robust to noise.

5. Conclusions

In this paper, the MPCM has been introduced for the construction of affine invariants, which can be viewed as the generalization of the traditional moment. The order of the traditional moment is generalized from integer to non-integer. In order to deal with the angular factor $\alpha(\theta)$ owing to shearing in affine transform, a repeated integral is directly employed to define the MPCM. The angular factor can easily be eliminated by using an appropriate repeated integral. As a result, non-integer order moments can be used to construct affine invariants. Based on the MPCM, a method for constructing affine invariants was provided. AMIs derived from traditional moments can be constructed by means of the proposed method with MPCMs. Furthermore, affine invariants can be constructed by any order MPCMs. Consequently, invariants constructed by real-order (less than 2) MPCMs can be derived. The experimental results demonstrated that these invariants are more robust to noise.

Although the order of the traditional moment has been generalized from integer to non-integer, the selection of an appropriate order is a problem that should be addressed, and will form our research direction in the future.

From Figs. 4(b) and 5, among others, we can observe that the robustness to noise of the constructed invariants first increases and then decreases when s_1 or s_2 varies from 1 to 4. This may be owing to the normalization by $M^4(2, 1, 0, 0)$ in Eq. (32). The further modification of MPCM is an additional research direction.

Acknowledgments

This work was supported in part by the National Natural Science Foundation of China, under Grants 61572015, 41375115, and 11301276.

Appendix A. Proofs of Theorems 2 and 3

Proof of Theorem 2

Proof. It follows from Eqs. (20) and (21) that $d\tilde{r} = \alpha(\theta)dr$ and

$$\tilde{\theta} = \arctan\frac{a_{21}\cos\theta + a_{22}\sin\theta}{a_{11}\cos\theta + a_{12}\sin\theta} = \arctan\beta(\theta).$$

Consequently,

$$\begin{aligned} d(\beta(\theta)) &= d\left(\frac{a_{21}\cos\theta + a_{22}\sin\theta}{a_{11}\cos\theta + a_{12}\sin\theta}\right) \\ &= \frac{a_{11}a_{22}\cos^2\theta + a_{11}a_{22}\sin^2\theta - a_{12}a_{21}\sin^2\theta - a_{12}a_{21}\cos^2\theta}{(a_{11}\cos\theta + a_{12}\sin\theta)^2}d\theta \\ &= \frac{a_{11}a_{22} - a_{12}a_{21}}{(a_{11}\cos\theta + a_{12}\sin\theta)^2}d\theta. \end{aligned}$$

We note that $det(A) = a_{11}a_{22} - a_{12}a_{21}$, and

$$1 + \beta(\theta)^2 = \frac{\alpha(\theta)^2}{(a_{11}\cos\theta + a_{12}\sin\theta)^2}.$$

Therefore,

$$d\tilde{\theta} = \frac{d\beta(\theta)}{1 + \beta(\theta)^2} = \frac{det(A)}{\alpha(\theta)^2}d\theta. \tag{33}$$

It follows from Eq. (22) that

$$\begin{aligned} &\sin(\tilde{\theta}_k - \tilde{\theta}_j) = \sin\tilde{\theta}_k\cos\tilde{\theta}_j - \cos\tilde{\theta}_k\sin\tilde{\theta}_j \\ &= \frac{(c\cos\theta_k + d\sin\theta_k)(a\cos\theta_j + b\sin\theta_j) - (c\cos\theta_j + d\sin\theta_j)(a\cos\theta_k + b\sin\theta_k)}{\alpha(\theta_k)\alpha(\theta_j)} \\ &= \frac{bc\cos\theta_k\sin\theta_j + ad\sin\theta_k\cos\theta_j - ad\cos\theta_k\sin\theta_j - bc\sin\theta_k\cos\theta_j}{\alpha(\theta_k)\alpha(\theta_j)} \\ &= \frac{det(A)}{\alpha(\theta_k)\alpha(\theta_j)}\sin(\theta_k - \theta_j). \end{aligned} \tag{34}$$

We note that

$$\begin{aligned} \tilde{M}(2,1,0,0) &= \int\left(\int \tilde{r}\tilde{f}(\tilde{r},\tilde{\theta})d\tilde{r}\right)d\tilde{\theta} \\ &= \int\int \alpha(\theta)rf(r,\theta)\alpha(\theta)\frac{det(A)}{\alpha^2(\theta)}drd\theta \\ &= det(A)M(2,1,0,0). \end{aligned}$$

Consequently,

$$\begin{aligned}\tilde{I} &= \frac{1}{\tilde{M}^n(2,1,0,0)}\int\int\cdots\int\prod_{i=1}^{g}\left|\int \tilde{r}_i^{s_i-1}\tilde{f}(\tilde{r}_i,\tilde{\theta}_i)d\tilde{r}_i\right|^{t_i}\\ &\quad\prod_{g\geq j>k\geq 1}\sin(\tilde{\theta}_k-\tilde{\theta}_j)^{m_{jk}}d\tilde{\theta}_1 d\tilde{\theta}_2\cdots d\tilde{\theta}_g\\ &= \frac{1}{(det(A))^n M^n(2,1,0,0)}\int\cdots\int\prod_{i=1}^{g}\left|\int(\alpha(\theta_i))r_i^{s_i-1}\alpha(\theta_i)f(r_i,\theta_i)dr_i\right|^{t_i}\\ &\quad\frac{(det(A))^{\sum_{g\geq j>k\geq 1}m_{jk}}(det(A))^g}{\prod_{i=1}^{g}\alpha^2(\theta_i)}\prod_{k,j=1}^{g}\left[\frac{\sin(\theta_k-\theta_j)}{\alpha(\theta_k)\alpha(\theta_j)}\right]^{m_{jk}}d\theta_1\cdots d\theta_g.\end{aligned}$$

It follows from Eqs. (23) and (24) that

$$\begin{aligned}\tilde{I} &= \frac{1}{M^n(2,1,0,0)}\int\int\cdots\int\prod_{i=1}^{g}\left|\int r_i^{s_i-1}f(r_i,\theta_i)dr_i\right|^{t_i}\\ &\quad\prod_{g\geq j>k\geq 1}\sin(\theta_k-\theta_j)^{m_{jk}}d\theta_1 d\theta_2\cdots d\theta_g = I.\end{aligned}$$

This completes the proof. □

Proof of Theorem 3

Proof. As m_{jk} $(j,k=1,\cdots,g)$ is a non-negative integer, $\sin(\theta_k-\theta_j)^{m_{jk}}$ can be obtained by the following equation:

$$[\sin(\theta_k-\theta_j)]^{m_{jk}}=\sum_{w=0}^{m_{jk}}(-1)^{m_{jk}-w}C_{m_{jk}}^{w}(\sin\theta_j\cos\theta_k)^w(\cos\theta_j\sin\theta_k)^{m_{jk}-w}.$$

Consequently, the quantity provided in Eq. (25) can be expressed in a polynomial of MPCMs.

$$\begin{aligned}I &= \frac{1}{M^n(2,1,0,0)}\int\int\cdots\int\prod_{i=0}^{g}\left|\int r_i^{s_i-1}f(r_i,\theta_i)dr_i\right|^{t_i}\prod_{g\geq j>k\geq 1}(-1)^{m_{jk}}\\ &\quad[\sin(\theta_2-\theta_1)]^{m_{21}}\cdots[\sin(\theta_g-\theta_1)]^{m_{g1}}[\sin(\theta_3-\theta_2)]^{m_{32}}\\ &\quad\cdots\ [\sin(\theta_g-\theta_2)]^{m_{g2}}\\ &\quad\cdots[\sin(\theta_g-\theta_{g-1})]^{m_{g(g-1)}}d\theta_1 d\theta_2\cdots d\theta_g\\ &= \frac{1}{M^n(2,1,0,0)}\int\int\cdots\int\prod_{i=0}^{g}\left|\int r_i^{s_i-1}f(r_i,\theta_i)dr_i\right|^{t_i}\\ &\quad\sum_{Q_{21}=0}^{m_{21}}C_{m_{21}}^{Q_{21}}[\sin\theta_1]^{Q_{21}}[\cos\theta_1]^{m_{21}-Q_{21}}[\sin\theta_2]^{m_{21}-Q_{21}}[\cos\theta_2]^{Q_{21}}(-1)^{Q_{21}+m_{21}}\cdots\\ &\quad\sum_{Q_{g1}=0}^{m_{g1}}C_{m_{g1}}^{Q_{g1}}[\sin\theta_1]^{Q_{g1}}[\cos\theta_1]^{m_{g1}-Q_{g1}}[\sin\theta_g]^{m_{g1}-Q_{g1}}[\cos\theta_g]^{Q_{g1}}(-1)^{Q_{g1}+m_{g1}}\\ &\quad\sum_{Q_{32}=0}^{m_{32}}C_{m_{32}}^{Q_{32}}[\sin\theta_2]^{Q_{32}}[\cos\theta_2]^{m_{32}-Q_{32}}[\sin\theta_3]^{m_{32}-Q_{32}}[\cos\theta_3]^{Q_{32}}(-1)^{Q_{32}+m_{32}}\cdots\\ &\quad\sum_{Q_{g2}=0}^{m_{g2}}C_{m_{g2}}^{Q_{g2}}[\sin\theta_2]^{Q_{g2}}[\cos\theta_2]^{m_{g2}-Q_{g2}}[\sin\theta_g]^{m_{g2}-Q_{g2}}[\cos\theta_g]^{Q_{g2}}(-1)^{Q_{g2}+m_{g2}}\cdots\\ &\quad\sum_{Q_{g(g-1)}=0}^{m_{g(g-1)}}C_{m_{g(g-1)}}^{Q_{g(g-1)}}[\sin\theta_{g-1}]^{Q_{g(g-1)}}[\cos\theta_{g-1}]^{m_{g(g-1)}-Q_{g(g-1)}}\\ &\quad[\sin\theta_g]^{m_{g(g-1)}-Q_{g(g-1)}}[\cos\theta_g]^{Q_{g(g-1)}}(-1)^{Q_{g(g-1)}+m_{g(g-1)}}d\theta_1 d\theta_2\cdots d\theta_g.\end{aligned}$$

It follows from Eq. (27), and (28) that

$$I=\frac{1}{M^n(2,1,0,0)}\left(\sum_{Q_{jk}=0}^{m_{jk}}\prod(-1)^{\sum(m_{jk}-Q_{jk})}C_{m_{jk}}^{Q_{jk}}\prod_{i=1}^{g}M(s_i,t_i,p_i,q_i)\right).$$

This completes the proof. □

Appendix B. Derivation of AMIs

In Section 3.3, we illustrate the derivation of *AMI*1 by means of Eq. (26). The derivation of AMI2 and AMI3 is provided below.

If we set $g=4, s_1=s_2=s_3=s_4=4$, $m_{21}=m_{43}=2$, and $m_{31}=m_{42}=1$, it follows from Eq. (26) that

$$\begin{aligned}AMI2 &= \frac{2}{M^{10}(2,1,0,0)}\big(-M^2(5,1,0,3)M^2(5,1,3,0)\\ &\quad+6M(5,1,0,3)\\ &\quad M(5,1,2,1)M(5,1,3,0)M(5,1,1,2)\\ &\quad-4M^3(5,1,2,1)M(5,1,0,3)\\ &\quad-4M^3(5,1,1,2)M(5,1,3,0)\\ &\quad+3M^2(5,1,2,1)M^2(5,1,1,2)\big).\end{aligned}$$

If we set $g=3, s_1=4, s_2=s_3=5$, $m_{21}=m_{31}=1$, and $m_{32}=2$, it follows from Eq. (26) that

$$\begin{aligned}AMI3 &= \frac{2}{M^7(2,1,0,0)}(M(4,1,0,2)M(5,1,1,2)M(5,1,3,0)\\ &\quad-M(4,1,0,2)M^2(5,1,2,1)\\ &\quad-M(4,1,1,1)M(5,1,0,3)M(5,1,3,0)\\ &\quad+4M(4,1,1,1)M(5,1,1,2)M(5,1,2,1)+M(4,1,2,0)\\ &\quad M(5,1,0,3)M(5,1,2,1)-M(4,1,2,0)M^2(5,1,1,2)\big).\end{aligned}$$

Supplementary material

Supplementary material associated with this article can be found, in the online version, at doi:10.1016/j.patcog.2018.07.036.

References

[1] K. Arbter, W.E. Snyder, H. Burkhardt, G. Hirzinger, Application of affine-invariant fourier descriptors to recognition of 3-d objects, IEEE Trans. Pattern Anal. Mach. Intell. 12 (7) (1990) 640–647.
[2] T.H. Reiss, The revised fundamental theorem of moment invariants, IEEE Trans. Pattern Anal. Mach. Intell. 13 (8) (1991) 830–834.
[3] Q.M. Tieng, W.W. Boles, Wavelet-based affine invariant representation: a tool for recognizing planar objects in 3 d space, IEEE Trans. Pattern Anal. Mach. Intell. 19 (8) (1997) 1287–1296.
[4] T. Suk, J. Flusser, B. Zitov, Moments and Moment Invariants in Pattern Recognition, John Wiley & Sons, 2009.
[5] D.S. Zhang, G.J. Lu, Review of shape representation and description techniques, Pattern Recognit. 37 (2004) 1–19.
[6] O. Tahri, A.Y. Tamtsia, Y. Mezouar, C. Demonceaux, Visual servoing based on shifted moments, IEEE Trans. Rob. 31 (3) (2015) 798–804.
[7] J. Flusser, T. Suk, J. Boldys, B. Zitovc, Projection operators and moment invariants to image blurring, IEEE Trans. Pattern Anal. Mach. Intell. 37 (4) (2015) 786–802.
[8] T. Suk, J. Flusser, J. Boldys, 3D rotation invariants by complex moments, Pattern Recognit. 48 (2015) 3516–3526.
[9] D. Bryner, E. Klassen, H. Le, A. Srivastava, 2D affine and projective shape analysis, IEEE Trans. Pattern Anal. Mach. Intell. 36 (5) (2014) 998–1011.
[10] B.W. Hong, S. Soatto, Shape matching using multiscale integral invariants, IEEE Trans. Pattern Anal. Mach. Intell. 37 (1) (2015) 151–160.
[11] M.R. Daliri, V. Torre, Robust symbolic representation for shape recognition and retrieval, Pattern Recognit. 41 (2008) 1782–1798.
[12] P.L.E. Ekombo, N. Ennahnahi, M. Oumsis, M. Meknassi, Application of affine invariant fourier descriptor to shape based image retrieval, Int. J. Comput. Sci. Netw. Secur. 9 (7) (2009) 240–247.
[13] X.B. Gao, C. Deng, X.L. Li, D.C. Tao, Geometric distortion insensitive image watermarking in affine covariant regions, IEEE Trans. Syst. Man Cybernet. Part C 40 (3) (2010) 278–286.
[14] M.I. Khalil, M.M. Bayoumi, A dyadic wavelet affine invariant function for 2d shape recognition, IEEE Trans. Pattern Anal.Mach. Intell. 23 (10) (2001) 1152–1163.
[15] M.I. Khalil, M.M. Bayoumi, Affine invariants for object recognition using the wavelet transform, Pattern Recognit. 23 (2002) 57–72.
[16] G. Liu, Z. Lin, Y. Yu, Radon representation-based feature descriptor for texture classification, IEEE Trans. Image Process 18 (5) (2009) 921–928.
[17] R. Matungka, Y.F. Zheng, R.L. Ewing, Image registration using adaptive polar transform, IEEE Trans. Image Process. 18 (10) (2009) 2340–2354.
[18] Y. Wang, E.K. Teoh, 2D affine-invariant contour matching using b-spline model, IEEE Trans. Pattern Anal. Mach. Intell. 29 (2007) 1853–1858.
[19] C. Teh, R. Chin, On image analysis by methods of moments, IEEE Trans. Pattern Anal. Mach. Intell. 10 (4) (1988) 496–513.

[20] M. Gruber, K.Y. Hsu, Moment-based image normalization with high noise-tolerance, IEEE Trans. Pattern Anal. Mach. Intell. 19 (2) (1997) 136–139.
[21] Y. Sheng, J. Duvernoy, Circular fourier-radial mellin descriptors for pattern recognition, J. Optical Soc. Am. A 3 (6) (1986) 885–888.
[22] L. Diao, J. Peng, J. Dong, F. Kong, Moment invariants under similarity transformation, Pattern Recognit. 48 (2015) 3641–3651.
[23] M.K. Hu, Visual pattern recognition by moment invariants, IRE Trans. Inform. Theory 8 (2) (1962) 179–187.
[24] S.A. Dudani, K.J. Breeding, R.B. McGhee, Aircraft identification by moment invariants, IEEE Trans. Comput. 26 (1) (1977) 39–45.
[25] Y.S. Abu-Mostafa, D. Psaltis, Recognitive aspects of moment invariants, IEEE Trans. Pattern Anal. Mach. Intell. 6 (6) (1984) 698–706.
[26] J. Flusser, T. Suk, Pattern recognition by affine moment invariants, Pattern Recognit. 26 (1) (1993) 167–174.
[27] T. Suk, J. Flusser, Affine moment invariants generated by graph method, Pattern Recognit. (2010), doi:10.1016/j.patcog.2010.05.015.
[28] H. Li, X. Jin, N. Yang, Z. Yang, The recognition of landed aircrafts based on pcnn model and affine moment invariants, Pattern Recognit. Lett. 51 (2014) 23–29.
[29] M. Gong, H. Li, W. Cao, Moment invariants to affine transformation of colours, Pattern Recognit. Lett. 34 (2014) 1240–1251.
[30] E. Rahtu, M. Salo, J. Heikkilä, Affine invariant pattern recognition using multiscale autoconvolution, IEEE Trans. Pattern Anal. Mach. Intell. 27 (2005) 908–918.
[31] Z. Yang, F. Cohen, Cross-weighted moments and affine invariants for image registration and matching, IEEE Trans. Pattern Anal. Mach. Intell. 21 (8) (1999) 804–814.
[32] E. Rahtu, M. Salo, J. Heikkil, J. Flusserä, Generalized affine moment invariants for object recognition, in: Proc 18th International Conference on Pattern Recognition (ICPR), 2, 2006, pp. 634–637.
[33] E. Rahtu, A multiscale framework for affine invariant pattern recognition and registration, 2007 Phd thesis.
[34] X. Wang, B. Xiao, J.F. Ma, X.L. Bi, Scaling and rotation invariant analysis approach to object recognition based on radon and fourier-mellin transforms, Pattern Recognit. 40 (2007) 3503–3508.
[35] T.V. Hoang, S. Tabbone, Invariant pattern recognition using the RFM descriptor, Pattern Recognit. 45 (2012) 271–284.
[36] T.V. Hoang, S. Tabbone, A geometric invariant shape descriptor based on the radon, fourier, and mellin transforms, in: International Conference on Pattern Recognition, 2010, pp. 2085–2088.
[37] L. Guo, M. Zhu, Quaternion fourier-mellin moments for color images, Pattern Recognit. 44 (2011) 187–195.
[38] J. Mennesson, C. Saint-Jean, L. Mascarilla, Color fourier-mellin descriptors for image recognition, Pattern Recognit. Lett. 40 (2014) 27–35.
[39] F. Bouyachchera, B. Boualia, M. Nasri, Clifford fourier-mellin moments and their invariants for color image recognition, Math. Comput. Simul. 40 (2014) 27–35.
[40] Hazewinkel, Michiel, Mellin Transform, Springer, 2001.
[41] http://www1.cs.columbia.edu/CAVE/software/softlib/coil20.php.
[42] http://www.image-net.org/challenges/LSVRC/2012.

Jianwei Yang received the M. S. degree in Mathematics from Xian Jiaotong University, and the Ph.D. degree in Computer Science from the Hong Kong Baptist University, Hong Kong, in 1996 and 2005 respectively. He is presently a Professor in the School of Mathematics and Statistics, Nanjing University of Information Science and Technology, Nanjing, China. His current research interests include pattern recognition, and computer vision.

Liang Zhang received the B. S. degree of Applied Mathematics from Nanjing University of Information Science and Technology, Nanjing, China in 2015. His current research interests include pattern recognition and computer vision.

Yuan Yan Tang received the Ph.D degree in Computer Science from Concordia University, Montreal, Canada. He is presently a chair professor in the Faculty of Science and Technology, University of Macau and a professor in the Department of Computer Science at Chongqing University. His current interests include wavelet theory and applications, pattern recognition, image processing, document processing, etc. He is the Founder and Editor-in-Chief of International Journal on Wavelets, Multiresolution, and Information Processing (IJWMIP). Professor Y. Y. Tang is an IAPR fellow and IEEE fellow.